Harmonizing Competing Intermediates: A Unified Free Energy Landscape of Protein RNase H

Ping Yu(余平)[1,2†], Zhenyong Xue(薛振勇)[3†], Hao Sun(孙皓)[2], Zhiqi Hou(侯志奇)[1,2], Zhuwei Zhang(张珠伟)[1,2], Yang Wang(王洋)[2], Shimin Le(乐世敏)[1*], and Hu Chen(陈虎)[1,2*]

[1]*Research Institute for Biomimetics and Soft Matter, Fujian Provincial Key Lab for Soft Functional Materials Research, Department of Physics, Xiamen University, Xiamen 361005, China*
[2]*Center of Biomedical Physics, Zhejiang Key Laboratory of Soft Matter Biomedical Materials, Wenzhou Institute, University of Chinese Academy of Sciences, Wenzhou 325000, China*
[3]*School of Electronic and Electrical Engineering, Shangqiu Normal University, Shangqiu 476000, China*

(Received 20 October 2025; accepted manuscript online 12 December 2025)

While single-domain proteins often exhibit two-state behavior, some proteins demonstrate complex folding pathways with intermediate states. Here, we investigate force-induced conformational transitions of RNase H using magnetic tweezers and reveal structurally distinct intermediate states in the folding and unfolding processes. Inspired by molecular dynamics simulations and verified by experiments on truncations, we found that the unfolding intermediate observed at forces above 8 pN represents a partially unfolded state with the C-terminal helix detached, while the folding intermediate observed below 6 pN corresponds to a partially folded state with only the core region formed, which is not the randomly collapsed molten globule state. Despite these structural differences, our comprehensive kinetic analysis demonstrates that both intermediates can be integrated into a unified quantitative free energy landscape along a single transition pathway. This reconciliation of competing folding intermediates provides fundamental insights into the complex dynamic behaviors of proteins in which different intermediate states are observed.

DOI: 10.1088/0256-307X/43/2/020901 CSTR: 32039.14.0256-307X.43.2.020901

Understanding the dynamics of protein folding and unfolding remains a major challenge due to its inherent stochastic properties,[1,2] influenced by functional and evolutionary constraints.[3,4] The folding process of many proteins is observed to be preceded by the formation of a partially structured conformation.[5,6] It is important to reveal whether the intermediates are on-pathway and productive to protein folding[7–9] or off-pathway and leading to misfolded states.[10,11] Traditional experimental methods struggle to precisely capture these transient and unstable intermediates,[12,13] single-molecule manipulation techniques offer substantial possibilities to reveal the detailed dynamic properties of conformational transitions with intermediates.[14,15]

Protein RNase H (RH) from *Escherichia coli* is an endonuclease crucial for maintaining genome stability.[16,17] It is a 155-residue single-domain protein with five α helices and five β strands.[18] In biochemical experiments, RH protein folds via a hierarchical mechanism, with the most stable core region folding first.[19,20] Rapid reversible transitions between the unfolded state and an intermediate state, assumed to be the molten globule state, were observed before successfully folding to the stable native state in optical tweezers experiments.[21] Steered molecular dynamics (SMD) simulations showed that the fifth α helix unfolds first under stretching force, followed by detachment of the first–third β strands.[22] The hierarchical folding mechanism and step-wise unfolding process make RH an ideal model protein for investigating protein dynamics with intermediates. Whether the folding and unfolding processes go through the same pathway and the character of free energy landscape remain elusive.

Here, we report a complete force-induced unfolding and refolding study of RH using magnetic tweezers (MT).[23,24] It is found that RH unfolds through an intermediate state and folds through another intermediate state with different step sizes and transition rates. MT experiments on truncations of RH and SMD simulations identify the possible conformations of the intermediate states. A unified free energy landscape along a single pathway is constructed to interpret the complex folding and unfolding dynamics of RH.

1. Unfolding and Folding Signals of RH. In MT experiments, the RH protein was site-specifically immobilized through dual anchoring: C-terminal SpyTag (St)-SpyCatcher (Sc) covalent conjugation and N-terminal biotin (bio)-streptavidin (SA) linkage to magnetic beads [Fig. 1(a)].[25,26] Initially, we conducted a force-ramp experiment as shown in Fig. 1(b). The stretching force was increased from 1 pN to 20 pN with a constant loading rate of 1 pN/s. We observed the unfolding signal of RH, which occurred in two consecutive steps from the native (N) state

†These authors contributed equally to this work.
*Corresponding authors. Email: leshimin@xmu.edu.cn; chenhu@xmu.edu.cn
© 2026 Chinese Physical Society and IOP Publishing Ltd. All rights, including for text and data mining, AI training, and similar technologies, are reserved.

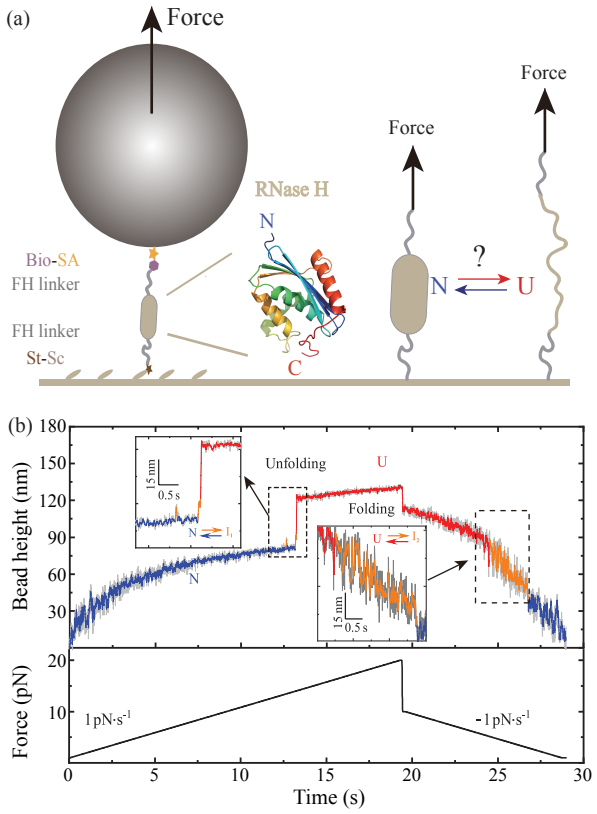

Fig. 1. Design of RH construct and typical data of force-ramp experiment by MT. (a) Schematic representation of RH stretching in MT. (b) In force-ramp experiment, force was increased from 1 pN to 20 pN with constant loading rate of 1 pN/s. Unfolding transition was observed at 13 pN passing through an intermediate state. Then force was dropped to 10 pN and decreased with constant loading rate of −1 pN/s. Folding precess was recorded at force range of 6–3 pN. Insets show the zoom-in figures of the unfolding and folding transitions.

to an intermediate (I) state and from I to the unfolded (U) state. Notably, the I state can also refold back to the N state. If the force is increased to more than 30 pN, the characteristic fingerprint signals of St-Sc can be detected,[27] confirming the correct protein tether [Fig. S1 of the Supplementary Materials (SM)].

After unfolding, force was dropped from 20 pN to 10 pN. The extension decreases from 122 nm to 110 nm due to the entropic elasticity of the polypeptide chain. Then we gradually reduced the force at a rate of −1 pN/s to record the folding process. Upon reaching a force range of 3–6 pN, we observed rapid reversible transitions between two states and subsequent stabilization at N state, which is consistent with previous optical tweezers experiments.[21] Therefore, we have observed the presence of intermediate states during both the folding and unfolding processes of RH at different force ranges in force-ramp experiments. It is crucial to determine whether these intermediate states represent the same conformation.

2. Step Size Statistics in Folding and Unfolding Processes. In force-ramp experiments, the explored force range with unfolding and folding transitions will change with varying loading rates. However, regardless of the loading rate, the explored force window remains constrained, and the transition events become rare at the extreme boundaries of this force range. To explore the transition dynamics at large force range, we measured the folding and unfolding transitions at different forces in force-jump experiments [Fig. 2(a)]. The process starts from the N state at low force, then the force was suddenly increased to 18 pN to induce the unfolding transition. After unfolding, the force is dropped to 3.5 pN to allow refolding. The experiment is repeated with unfolding forces between 6 and 18 pN and folding forces between 3.5 and 5.5 pN. The transitions between the N and I states were recorded during the unfolding processes, and the rapid reversible transitions between the U and the folding I state were observed before stabilizing at the N state.

Multiple cycles of unfolding and folding measurements produce enough data for statistical analysis. We integrated all measured bead height data at the same constant force into a dataset. Distribution histograms of the combined bead heights are fitted with a three-peak Gaussian function (Figs. S2 and S3 of the SM). The three peaks were identified as three different protein states: the highest bead height peak signifies the U state, the intermediate peak represents the I state (specifically I_1 for unfolding and I_2 for folding), and the lowest peak corresponds to the N state.

Through the distance between the peaks, we determined the step sizes of different transitions: the transitions from N to I_1 [$\Delta x_{NI_1}(F)$], I_1 to U [$\Delta x_{I_1U}(F)$], and N to U [$\Delta x_{NU}(F)$] during protein unfolding, as well as the transitions from U to N [$\Delta x_{UN}(F)$], U to I_2 [$\Delta x_{UI_2}(F)$], and I_2 to N [$\Delta x_{I_2N}(F)$] during the folding process [Fig. 2(b)]. We found that $\Delta x_{UI_2}(F)$ is approximately equal to $\Delta x_{I_2N(F)}$, which indicates that about half of RH folds in the I_2 state. The dashed red line represents the fitting curve of the extension difference between N and U states using worm-like chain (WLC) model [Eq. (S1) of the SM] with contour length of $\Delta L_{NU} = 52.8$ nm and persistence length of 0.8 nm. To guide the eye, dashed curves are WLC curves with different contour lengths and the same persistence length to fit $\Delta x_{NI_1}(F)$ ($\Delta L_{NI_1} = 11.6$ nm), $\Delta x_{I_1U}(F)$ ($\Delta L_{I_1U} = 42.6$ nm), and $\Delta x_{UI_2}(F)$ [$\Delta x_{I_2N}(F)$] ($\Delta L_{UI_2} = \Delta L_{I_2N} = 27.1$ nm). The different contour lengths of ΔL_{NI_1} and ΔL_{I_2N} show that intermediate states I_1 and I_2 represent two structurally distinct conformations.

3. Apparent Force-Dependent Folding and Unfolding Rates. To roughly quantify the dynamics, we ignore the I states and focus on the apparent folding and unfolding rates of RH. The total time required to unfold from N to U (t_{NU}) and that required to fold from U to N (t_{UN}) at each constant force [Fig. 2(a)] are analyzed using single-exponential fittings [Figs. S4 and S5 of the SM] to obtain the force-dependent apparent unfolding rate $k_u^{app}(F)$ and folding rate $k_f^{app}(F)$ [black symbols in Figs. 2(c), 2(d), and Fig. S6 of the SM].

4. Detailed Transition Rates in the Unfolding Process. As shown in Fig. 2(a), the force applied on the protein in the native state was suddenly increased to induce the unfolding transition. The protein can unfold through the I_1 state, and I_1 can also fold back to the N state. We denote

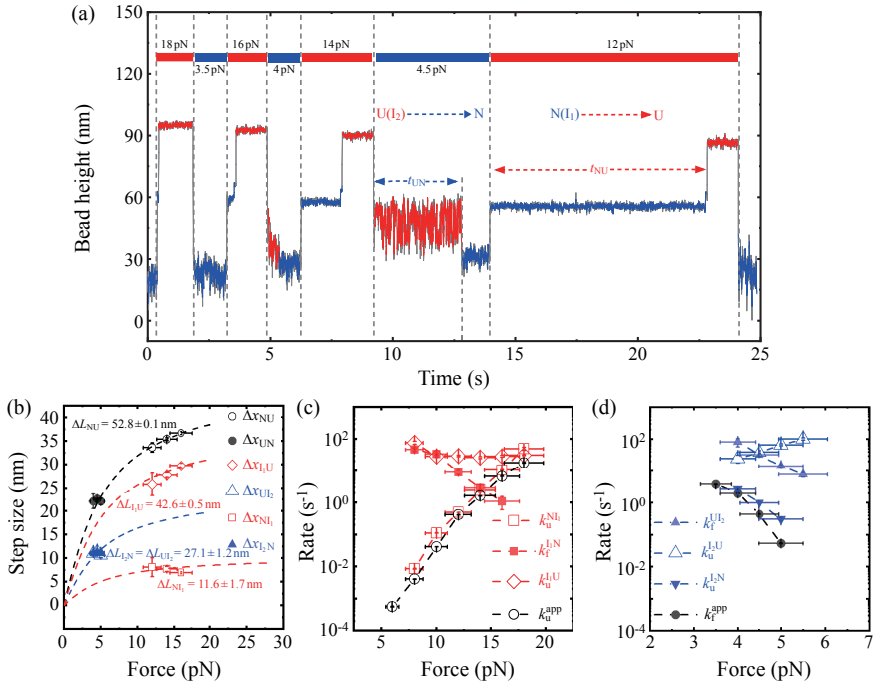

Fig. 2. Force-jump experiments and force-dependent unfolding and folding process involving N, I_1, I_2, and U states of RH. (a) Typical force-jump experiments show the unfolding process at 12–18 pN and folding process at 3.5–4.5 pN. (b) The force-dependent step sizes of the folding transitions and unfolding transitions. (c) Force-dependent transition rates k_u^{app}, $k_u^{NI_1}$, $k_f^{I_1N}$, and $k_u^{I_1U}$ of RH during the unfolding process. (d) Force-dependent transition rates k_f^{app}, $k_f^{UI_2}$, $k_u^{I_2U}$, and $k_f^{I_2N}$ of RH during the folding process. All results are obtained from statistical analysis of data from more than three independent tethers. The uncertainty of force is estimated as 10%.

the time the protein spends in N state and I_1 state as t_N and t_{I_1}, respectively. By performing a single-exponential fitting to the survival probabilities of N and I_1, the lifetimes of N (τ_N) and I_1 (τ_{I_1}) can be obtained (Fig. S7 of the SM). The transition rate from N to I_1 is $k_u^{NI_1} = 1/\tau_N$, while the transition rates $k_f^{I_1N}(F)$ and $k_u^{I_1U}(F)$ can be obtained from τ_{I_1} and the count ratio of transitions $I_1 \to$N and $I_1 \to$U (Fig. S7 of the SM).[9]

Figure 2(c) shows the transition rates between the N, I_1, and U states during unfolding, measured at various forces. Both $k_f^{I_1N}$ and $k_u^{NI_1}$ are sensitive to force, while $k_u^{I_1U}$ is $\sim 28\,s^{-1}$ and almost independent of force. The intersection of $k_f^{I_1N}(F)$ and $k_u^{NI_1}(F)$ delineates a critical force $F_c^{NI_1}$ of 14.4 pN, corresponding to a free energy difference of 19.1 k_BT between N and I_1 [Eq. (S3) of the SM].

5. Detailed Transition Rates in the Folding Process. The folding process of RH can be described as U $\rightleftharpoons$ I_2 $\to$ N. Figure S8(a) of the SM shows the folding process at 5 pN in three cycles of measurements on the same protein tether. Histogram of the bead height can be fitted with a three-peak Gaussian function. The ratio of the areas of the peaks of U and I_2 gives the ratio of the probabilities of U and I_2 which is equal to $k_u^{I_2U}(F)/k_f^{UI_2}(F)$. Furthermore, the autocorrelation function of the time course during the fluctuation between U and I_2 shows an exponential decay curve with relaxation rate equal to $k_u^{I_2U}(F) + k_f^{UI_2}(F)$ [Fig. S8(b) of the SM].[29] Therefore, $k_u^{I_2U}(F)$ and $k_f^{UI_2}(F)$ can be determined in the protein folding process. The intersection of $k_u^{I_2U}(F)$ and $k_f^{UI_2}(F)$ gives a critical force $F_c^{I_2U}$ of 4.4 pN, corresponding to a free energy difference of 6.7 k_BT between U and I_2.

We can further get the folding rate from I_2 to N [$k_f^{I_2N}(F)$] using the equation[29]

$$k_f^{app}(F) = \frac{k_f^{I_2N}(F)k_f^{UI_2}(F)}{k_f^{I_2N}(F) + k_f^{UI_2}(F) + k_u^{I_2U}(F)} \quad (1)$$

with the measured $k_u^{I_2U}(F)$, $k_f^{UI_2}(F)$, and $k_f^{app}(F)$ [Fig. 2(d)].

6. SMD Simulations of RH. In SMD simulation, the fifth α helix of RH protein unfolds initially, followed by the subsequent unfolding of the 1–3 β strands at N-terminus [Fig. 3(a)], which is consistent with previous studies.[22] From the extension x and forces f, the corresponding contour length L is obtained through the WLC model with persistence length $A = 0.4$ nm [Eq. (S2) of the SM].[30] The probability distribution of L was fitted with an 8-peak Gaussian function [Fig. 3(b)]. Solid curves show the experimentally observed four states, including the N state ($L_N = 6.6 \pm 1.2$ nm), I_1 ($L_{I_1} = 16.6 \pm 0.5$ nm), I_2 ($L_{I_2} = 36.3 \pm 3.6$ nm), and U state ($L_U = 57.4 \pm 1.0$ nm). The contour lengths of these four states give rise to step sizes similar to those in the experimental data. Dashed peaks indicate metastable states observed in simulations but not experimentally resolved. To guide the eye, the theoretical force-extension curves [Eq. (S2) of the SM] of WLC models with contour lengths of 6.6, 16.6, 36.3, and 57.4 nm and a common persistence length $A = 0.4$ nm are plotted as black curves in the force range of simulation [Fig. 3(a)].

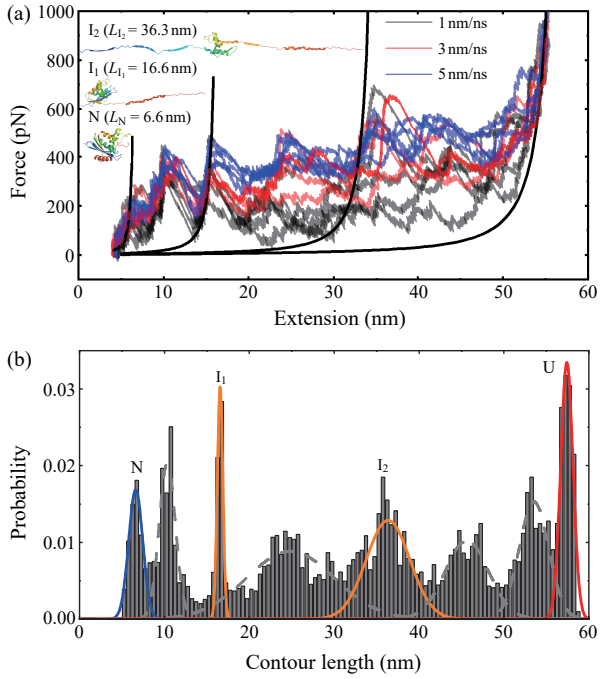

Fig. 3. SMD simulations of RH unfolding. (a) The black, red, and blue curves represent trajectories from SMD simulations where the C-terminus of RH was pulled via a harmonic spring with spring constant 100 kJ/mol/nm^2 at velocities of 1, 3, and 5 nm/ns, respectively. For each pulling speed, five independent replicas were performed to assess reproducibility. Thick black curves are theoretical force-extension curves of the WLC model with contour lengths of 6.6, 16.6, 36.3, and 57.4 nm, respectively. Insets show the snapshots of the N, I_1, and I_2 states. (b) Probability distribution of contour lengths (L) derived from simulations is fitted with eight Gaussian functions. The blue peak represents the N state ($L_N = 6.6$ nm), while orange and red peaks correspond to the intermediate (I_1, $L_{I_1} = 16.6$ nm; I_2, $L_{I_2} = 36.3$ nm) and the U states ($L_U = 57.4$ nm), respectively. Dashed peaks indicate metastable states observed in simulations but not experimentally resolved.

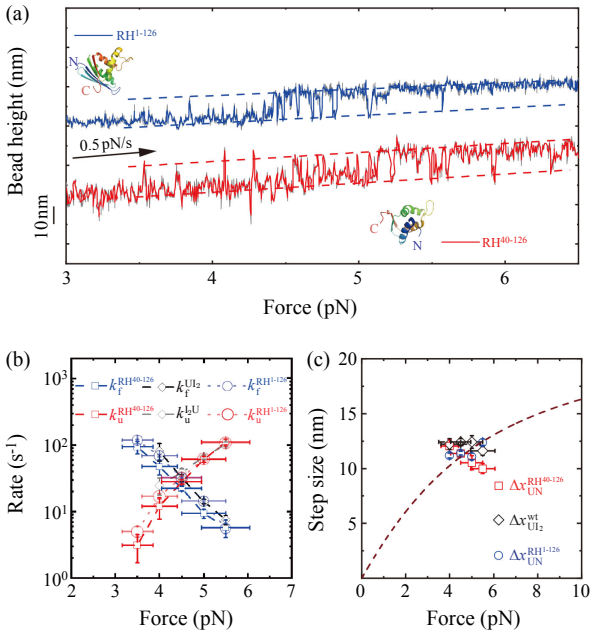

Fig. 4. Unfolding and folding dynamics of truncations RH^{1-126} and RH^{40-126} measured by MT. (a) In the force-ramp experiment with a constant loading rate of 0.5 pN/s, reversible unfolding and folding events were observed at 4–5.5 pN for both RH^{1-126} and RH^{40-126}. Insets show the structures of both truncations. (b) Force-dependent unfolding rates (red) and folding rates (blue) of RH^{1-126} and RH^{40-126} obtained from equilibrium constant-force experiments align well with the transition rates (black) between U and I_2 of the wild-type RH. (c) Step sizes of RH^{40-126} (red) and RH^{1-126} (blue) are consistent with those between U and I_2 (black) of the wild-type RH. The dashed curve represents the theoretical step size of RH^{40-126} assuming it unfolds in a single step. The uncertainty of force is estimated as 10%.

7. Measurements on the Truncated RH by MT. Inspired by the SMD simulation results, we assume that I_1 has the C-terminal part unfolded, and I_2 has both the C- and N-terminal parts unfolded. Two truncations of RH are designed and studied in MT experiments to test this hypothesis: RH^{1-126} has 29 C-terminal residues removed, and RH^{40-126} has an additional 39 N-terminal residues removed.

In force-ramp experiments of two truncations RH^{1-126} and RH^{40-126}, force is increased from 3 to 7 pN at a constant loading rate. The same reversible unfolding and folding events were observed at 4–5.5 pN for both truncations [Fig. 4(a) and Figs. S9 and S10 of the SM]. Force-dependent folding and unfolding rates of RH^{1-126} and RH^{40-126} are obtained by constant-force experiments, and they agrees with the reversible transitions between U and I_2 of RH [Fig. 4(b)]. Despite the transition rates, the unfolding step sizes of RH^{1-126} and RH^{40-126} are also consistent with those between U and I_2 states of wild-type RH in the same force range of 4–5.5 pN [Fig. 4(c)], which agrees with theoretical step size of RH^{40-126} and is much shorter than that of RH^{1-126}. It indicates that only the core region forms a well-defined structure while the N-terminal part of RH^{1-126} remains unfolded.

8. Slow Unfolding of RH below 6 pN. Taking advantage of the stability of MT, we captured the unfolding events of RH at low forces of 4–6 pN by applying forces for a long duration of several hours (Fig. S11 of the SM). After unfolding, rapid reversible fluctuations between I_2 and U were observed. Therefore, the lifetime of N at 4–6 pN gives the slow unfolding rate $k_u^{NI_2}$ on the order of $\sim 10^{-4}$ s^{-1} shown in Fig. 5(a).

9. Arrhenius Fitting of Folding and Unfolding Rates. All transition rates involving N, I_1, I_2, and U are summarized in Fig. 5(a) and can be fitted with Arrhenius' formula[31,32] [see Eqs. (S4) and (S5) of SM] to obtain the zero-force transition rate (k_{u0} or k_{f0}) and the contour length difference between the initial state and the transition state (ΔL_{x_u} or ΔL_{x_f}) with superscript indicating the initial state and the target state. The corresponding parameters are $\Delta L_{x_u}^{NI_1} = 5.6 \pm 0.4$ nm, $k_{u0}^{NI_1} = 3.5 \times 10^{-4}$ s^{-1}, $\Delta L_{x_f}^{I_1N} = 3.0 \pm 0.9$ nm, $k_{f0}^{I_1N} = 450$ s^{-1}, $\Delta L_{x_f}^{UI_2} = 14.7 \pm 1.5$ nm, $k_{f0}^{UI_2} = 1400$ s^{-1}, $\Delta L_{x_u}^{I_2U} = 9.4 \pm 0.3$ nm, $k_{u0}^{I_2U} = 3.5$ s^{-1}, $\Delta L_{x_f}^{I_2N} = 21.8 \pm 1.3$ nm, $k_{f0}^{I_2N} = 250$ s^{-1}, $\Delta L_{x_u}^{NI_2} = 11.8 \pm 2.0$ nm, and $k_{u0}^{NI_2} = 4.1 \times 10^{-6}$ s^{-1}.

The intersection of the extrapolated $k_f^{I_2N}(F)$ and $k_u^{NI_2}(F)$ gives a critical force $F_c^{NI_2}$ of $\sim$7 pN, corresponding to a free energy difference of $\sim 14.7\, k_BT$ between N and I_2 [Eq. (S3) of the SM].

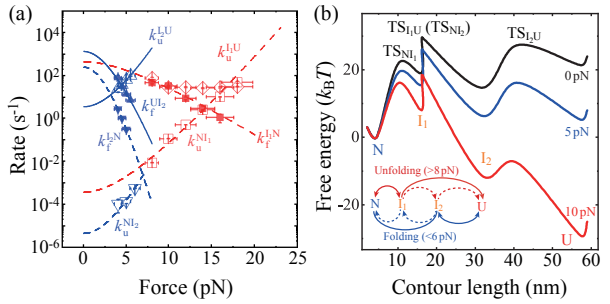

Fig. 5. Data analysis and unified free energy landscape of RH. (a) Force-dependent transition rates of RH: $k_u^{NI_1}$, $k_f^{I_1N}$, $k_u^{I_1U}$ at forces greater than 8 pN and $k_u^{I_2U}$, $k_f^{UI_2}$, $k_u^{NI_2}$, $k_f^{I_2N}$ at forces smaller than 6 pN are fitted using the Arrhenius formula. (b) The free energy landscape of RH constructed based on the force-dependent transition rates, including two distinct intermediate states. The black, blue, and red curves represent the free energy landscapes under forces of 0 pN, 5 pN, and 10 pN, respectively. The inset illustrates the folding and unfolding processes of RH, where solid curved arrows denote experimentally observed transitions, while dashed curved arrows indicate the underlying actual processes.

10. Free Energy Landscape of RH. RH unfolds through I_1 at forces >8 pN and refolds through I_2 at forces <5.5 pN. The most intuitive model is that RH unfolds through a pathway and folds through another pathway. But detailed analysis shows that a simpler model with a single transition pathway can describe the experimental results. Linear extrapolations show that $k_u^{I_2U}(F)$ and $k_f^{I_1N}(F)$ are much faster than our sampling rate at forces >8 pN and <5.5 pN, respectively [Fig. 5(a)]. We did not detect I_2 in the unfolding process at forces >8 pN and I_1 in the folding process at forces <5.5 pN due to their short lifetimes. Therefore, a one-dimensional energy landscape with N, I_1, I_2, and U states is constructed along the reaction coordinate of the contour length with the free energy of N as the reference [Fig. 5(b)].

From the step size of transitions [Fig. 2(b)] and the N-C distance of N state, the contour lengths of N, I_1, I_2, and U states can be estimated to be 4.5 nm, 16.1 nm, 31.6 nm, and 57.3 nm, respectively. From the critical forces of $F_c^{NI_1}$, $F_c^{NI_2}$, and $F_c^{I_2U}$, the free energies of I_1, I_2, and U are determined as 19.1 k_BT, 14.7 k_BT, and 21.4 k_BT, respectively. The locations of barriers can be estimated from the fitting parameters $\Delta L_{x_u}^{NI_1}$, $\Delta L_{x_u}^{NI_2}$, and $\Delta L_{x_u}^{I_2U}$. As the unfolding rate $k_u^{I_1U} \sim 28\,s^{-1}$ is almost independent of force, it gives an unfolding barrier very close to I_1. The coincidence of the highest barrier between N and I_2 and the one between I_1 and U indicates that the barriers (or transition states) TS_{NI_2} and TS_{I_1U} are the same.

The barrier height $\Delta G^{\ddagger}$ can be estimated by an empirical equation of the zero-force transition rate: $k_0 = k^* \exp(-\Delta G^{\ddagger}/k_BT)$ where k^* is the intrinsic transition rate of $10^6\,s^{-1}$ without barrier.[33] Therefore, the barrier heights $\Delta G_{NI_1}^{\ddagger} = 21.8\,k_BT$, $\Delta G_{I_1U}^{\ddagger} = 10.5\,k_BT$, $\Delta G_{NI_2}^{\ddagger} = 26.2\,k_BT$, and $\Delta G_{I_2U}^{\ddagger} = 12.6\,k_BT$. Considering the free energies of I_1 and I_2, the free energies of the transition states with N as reference can be obtained. Figure 5(b) shows the free energy landscape at zero force together with those at 5 and 10 pN to interpret the force-dependent folding and unfolding processes of RH.

In summary, we examined the conformational transitions of RH under stretching forces applied between its N- and C-termini over a force range from 3.5 to 18 pN using MT. RH unfolds through an intermediate state I_1 when the force increases to higher than 8 pN, while the unfolded RH folds via another intermediate state I_2 when the stretching force decreases to lower than 6 pN. All possible force-dependent transition rates are determined. Distinct step sizes and dynamic properties show that I_1 and I_2 have different conformations. Inspired by the SMD simulations, the unfolding intermediate state I_1 might have only the C-terminal helix destroyed in the unfolding process at forces >8 pN. A similar folding intermediate state was observed in an optical tweezers experiment,[21] and it was explained as the molten globule state[34,35] with a collapsed dynamic conformation of the full-length polypeptide. Our measurements of the RH truncation show the same reversible transitions as those between U and I_2 in the folding process of full-length RH, showing that I_2 is a partially folded state with the core region formed and both N- and C-terminal parts unstructured, contrasting sharply with the molten globule state with a fluctuating collapsed random conformation and poorly defined tertiary packing.

Though different intermediate states are observed in the folding and unfolding processes, they can exist on the same transition pathway. The appearance of each intermediate state is determined by the initial state and the value of stretching forces. Along a single pathway, a unified free energy landscape with N, I_1, I_2, and U states is constructed to describe all experimental results. Theoretically, protein dynamics are in a multi-dimensional conformational space. The transition pathways along one or more reaction coordinates are all simplified models to interpret the experimental observations. Though the intuitive two-pathway model cannot be ruled out, our single pathway model is strongly supported as the simplest framework that quantitatively interprets all experimental results. Our study provides new insights into the complex dynamic behaviors of proteins in which different intermediate states play a pivotal role in different dynamic processes.

Acknowledgements. This work was supported by the National Natural Science Foundation of China (Grant Nos. 12474200, 12174322 to HC, 32541047, 32271367, 12204389 to SL), the 111 project (Grant No. B16029), and the Research Fund of Wenzhou Institute (Grant No. WIUCASQD2021008).

References

[1] Dobson C M 2003 *Nature* **426** 884
[2] Dill K A and MacCallum J L 2012 *Science* **338** 1042
[3] Debes C, Wang M, Caetano-Anolles G, and Grater F 2013 *PLOS Comput. Biol.* **9** e1002861
[4] Kocher C D and Dill K A 2024 *Proc. Natl. Acad. Sci. U.S.A.* **121** e2315000121
[5] Sen Mojumdar S, Scholl Z N, Dee D R, Rouleau L, Anand U, Garen C, and Woodside M T 2017 *Nat. Commun.* **8** 1881

[6] Foroutannejad S, Good L L L, Lin C, Carter Z I I, Tadesse M G G, Lucius A L L, Crane B R R, and Maillard R A A 2023 *Nat. Commun.* **14** 1057

[7] Garcia-Manyes S, Dougan L, Badilla C L, Brujic J, and Fernandez J M 2009 *Proc. Natl. Acad. Sci. U.S.A.* **106** 10534

[8] Yu H, Siewny M G W, Edwards D T, Sanders A W, and Perkins T T 2017 *Science* **355** 945

[9] Sun H, Guo Z L, Hong H Y, Zhang Z W, Zhang Y H, Wang Y, Le S M, and Chen H 2023 *Phys. Rev. Lett.* **131** 218402

[10] Yu H, Liu X, Neupane K, Gupta A N, Brigley A M, Solanki A, Sosova I, and Woodside M T 2012 *Proc. Natl. Acad. Sci. U.S.A.* **109** 5283

[11] Xu J S, Sun H, Zhang Z W, Guo Z L, Le S M, and Chen H 2024 *J. Phys. Chem. Lett.* **15** 11954

[12] Dabora J M and Marqusee S 1994 *Protein Sci.* **3** 1401

[13] Fersht A R 2000 *Proc. Natl. Acad. Sci. U.S.A.* **97** 14121

[14] Guo Z L, Hong H Y, Yuan G H, Qian H, Li B, Cao Y, Wang W, Wu C X, and Chen H 2020 *Phys. Rev. Lett.* **125** 198101

[15] Jacobson D R, Uyetake L, and Perkins T T 2020 *Biophys. J.* **118** 667

[16] Schultz S J and Champoux J J 2008 *Virus Res.* **134** 86

[17] Lockhart A, Pires V B, Bento F, Kellner V, Luke-Glaser S, Yakoub G, Ulrich H D, and Luke B 2019 *Cell Rep.* **29** 2890

[18] Katayanagi K, Miyagawa M, Matsushima M, Ishikawa M, Kanaya S, Nakamura H, Ikehara M, Matsuzaki T, and Morikawa K 1992 *J. Mol. Biol.* **223** 1029

[19] Raschke T M and Marqusee S 1997 *Nat. Struct. Biol.* **4** 298

[20] Raschke T M, Kho J, and Marqusee S 1999 *Nat. Struct. Biol.* **6** 825

[21] Cecconi C, Shank E A, Bustamante C, and Marqusee S 2005 *Science* **309** 2057

[22] Schmitt T J, Clark J E, and Knotts IV T A 2009 *J. Chem. Phys.* **131** 235101

[23] Chen H, Fu H X, Zhu X Y, Cong P W, Nakamura F, and Yan J 2011 *Biophys. J.* **100** 517

[24] Tapia-Rojo R, Mora M, and Garcia-Manyes S 2024 *Nat. Protoc.* **9** 1

[25] Hong H Y, Guo Z L, Sun H, Yu P, Su H H, Ma X N, and Chen H 2021 *Commun. Chem.* **4** 156

[26] Ma X N, Sun H, Hong H Y, Guo Z L, Su H H, and Chen H 2022 *Phys. Rev. E* **106** 024404

[27] Guo Z L, Hong H Y, Sun H, Zhang X F, Wu C X, Li B, Cao Y, and Chen H 2021 *Nanoscale* **13** 11262

[28] Zoldak G, Stigler J, Pelz B, Li H B, and Rief M 2013 *Proc. Natl. Acad. Sci. U.S.A.* **110** 18156

[29] Pierse C A and Dudko O K 2017 *Phys. Rev. Lett.* **118** 088101

[30] Rief M, Gautel M, Oesterhelt F, Fernandez J M, and Gaub H E 1997 *Science* **276** 1109

[31] Chen H, Yuan G H, Winardhi R S, Yao M X, Popa I, Fernandez J M, and Yan J 2015 *J. Am. Chem. Soc.* **137** 3540

[32] Rognoni L, Stigler J, Pelz B, Ylanne J, and Rief M 2012 *Proc. Natl. Acad. Sci. U.S.A.* **109** 19679

[33] Best R B and Hummer G 2006 *Phys. Rev. Lett.* **96** 228104

[34] Elms P J, Chodera J D, Bustamante C, and Marqusee S 2012 *Proc. Natl. Acad. Sci. U.S.A.* **109** 3796

[35] Tapia-Rojo R, Eckels E C, and Fernandez J M 2019 *Proc. Natl. Acad. Sci. U.S.A.* **116** 7873